ACS NANOSCIENCE Au
AN OPEN ACCESS JOURNAL OF THE AMERICAN CHEMICAL SOCIETY

Open Access
This article is licensed under CC-BY-NC-ND 4.0

pubs.acs.org/nanoau
Article

Formation of Iron Phosphide Nanobundles from an Iron Oxyhydroxide Precursor

Menuka Adhikari,[†] Shubham Sharma,[†] Elena Echeverria, David N. McIlroy, and Yolanda Vasquez*

Cite This: ACS Nanosci. Au 2023, 3, 491−499
Read Online

ACCESS | Metrics & More | Article Recommendations | Supporting Information

ABSTRACT: Iron phosphide (FeP) nanoparticles have excellent properties such as fast charge transfer kinetics, high electrical conductivity, and high stability, making them a promising catalyst for hydrogen evolution reaction (HER). A challenge to the wide use of iron phosphide nanomaterials for this application is the available synthesis protocols that limit control over the resulting crystalline phase of the product. In this study, we report a method for synthesizing FeP through a solution-based process. Here, we use iron oxyhydroxide (β-FeOOH) as a cost-effective, environmentally friendly, and air-stable source of iron, along with tri-*n*-octylphosphine (TOP) as the phosphorus source and solvent. FeP is formed in a nanobundle morphology in the solution phase reaction at a temperature of 320 °C. The materials were characterized by pXRD and transmission electron microscopy (TEM). The optimization parameters evaluated to produce the phosphorus-rich FeP phase included the reaction rate, time, amount of TOP, and reaction temperature. Mixtures of Fe_2P and FeP phases were obtained at shorter reaction times and slow heating rates (4.5 °C /min), while longer reaction times and faster heating rates (18.8 °C/min) favored the formation of phosphorus-rich FeP. Overall, the reaction lever that consistently yielded FeP as the predominant crystalline phase was a fast heat rate.

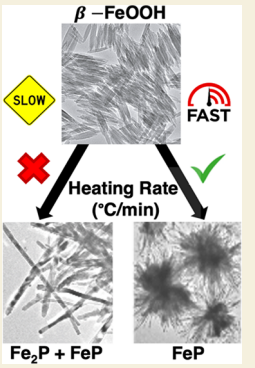

KEYWORDS: *Iron oxyhydroxide, Iron phosphide, Nanobundles, Heating rate, Solution synthesis*

INTRODUCTION

Nanoscale transition metal phosphides (TMPs) are an important class of materials due to their wide scope of interesting applications ranging from lithium−ion battery anodes,[1] absorbers in photovoltaics,[2] supercapacitors,[3] magnetic sensors,[4] and catalysts in numerous processes that include hydroprocessing, water−gas−shift reactions, and water splitting.[5−9] Iron phosphides alone have shown remarkable activity as catalysts for water-splitting reactions.[10−12] Compounds of iron and phosphorus exhibit a range of compositions that include FeP, Fe_3P, Fe_2P, FeP_4, and FeP_2, and their nonstoichiometric variations, which allow for modulation of their resultant properties by their respective electronic and physical attributes.[13,14] For example, CoP@FeP_4 composites are promising electrode systems for dye-sensitized solar cells.[15] Another iron phosphide phase, FeP, exhibits superior electrocatalytic activity towards overall water splitting.[16−20] Additionally, studies have shown that iron phosphide (FeP) is a good choice for reversible electrodes in lithium−ion and sodium−ion batteries and thermoelectric materials.[21−25] As such, several studies have focused on synthetic strategies to generate iron phosphides with a precise chemical composition and morphology.

Our work aims to synthesize phase pure FeP for its potential use as an electrode material for lithium- and sodium-ion batteries (LIBs and NaBs). Iron phosphide (FeP) nanomaterials exhibit physical properties, such as a high insertion/extraction coefficient of Na/Li ions, good cyclic stability, and rate capability, making them promising electrode materials for lithium- and sodium-ion batteries. Synthetic approaches for producing FeP nanomaterials include the high-temperature annealing of organometallic and solid-state precursors,[26−28] solvothermal reactions,[29] the co-reaction of metal−organic frameworks with phosphines,[30,31] the decomposition of single source precursors,[32] microwave synthesis,[33] high energy ball milling,[34] and metal-organic chemical vapor deposition.[14] However, these methods lack significant control over morphology and tend to result in agglomerated nanoparticles.[35] A well-developed solution-based approach for synthesizing FeP includes the reaction of iron salt precursors with a mixture of tri-*n*-octylphosphine (TOP) and trioctylphosphine oxide (TOPO) in the presence of aliphatic amines at high temperatures. This strategy was reported by Brock and co-workers for the synthesis of FeP by the reaction of $Fe(acac)_3$ with $P(SiMe_3)_3$ in TOPO at 280 °C.[27] In this method, high reaction temperatures are used to cleave the strong P−C bond, resulting in the release and diffusion of phosphorus within the metal particulates. Researchers have used variations of this wet-chemical method to synthesize FeP

Received: July 29, 2023
Revised: October 18, 2023
Accepted: October 19, 2023
Published: November 8, 2023

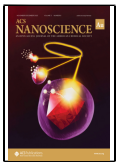

© 2023 The Authors. Published by American Chemical Society

https://doi.org/10.1021/acsnanoscienceau.3c00036
ACS Nanosci. Au 2023, 3, 491−499

Scheme 1. Basic Synthetic to Generate Fe_xP Nanobundles

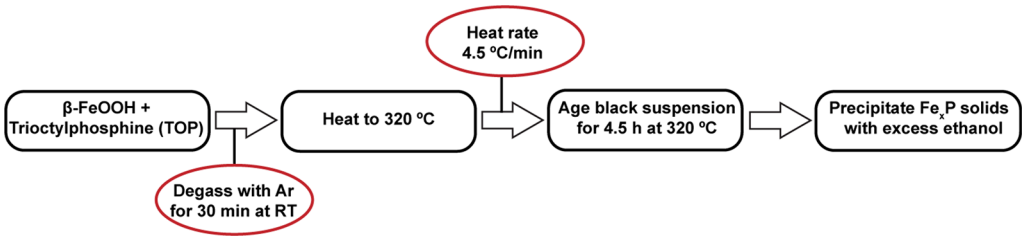

nanoparticles using commercially available iron precursors such as $Fe(CO)_5$, $Fe(acac)_3$, and $Fe(N(SiMe_3)_2)_3$. However, some of these iron compounds are fire hazardous and require safety precautions. Some studies have used different phosphine substituents as a source of phosphorus.[36] For instance, Chen and co-workers also conducted a study where they synthesized FeP nanowires through the catalytic cleavage of the P−C bond caused by reacting TOP with nanocrystalline Fe at high temperatures.[31,45] Similarly, Hyeon and co-workers reported the synthesis of FeP and Fe_2P nanorods via continuous injection of $Fe(CO)_5$ and TOP into hot surfactant/solvent systems.[7,28] Likewise, Henkes, Vasquez, and Schaak reported the transformation of various transition metal nanoparticles to their respective phosphide analogues.[37−40] Specifically, FeP nanoparticles were synthesized by reacting $Fe(acac)_3$ with TOP in hexadecyl amine at 360 °C.[39] Despite promising results, research on alternative and readily available iron precursors remains limited.

In this work, we utilize iron oxyhydroxide (β-FeOOH) as a cost-effective and convenient iron precursor for the wet-chemical synthesis of FeP. Only two literature reports use β-FeOOH as a precursor for the synthesis of FeP to the best of our knowledge. Both studies use traditional high-temperature solid-phase phosphidation.[41,42] However, our study is the first to document the solution synthesis of FeP nanoparticles using β-FeOOH nanorods. The synthesis method involves reacting β-FeOOH nanorods with TOP as an iron and phosphorus source, respectively, at 320 °C. This process generates phosphorus in situ by the catalytic cleavage of the P−C bond of TOP at elevated temperatures, similar to the protocols already discussed. Furthermore, we explore the impact of various synthetic parameters, such as reaction time, temperature, precursor concentration, and heating rate, on the formation of phase pure FeP nanoparticles.

RESULTS AND DISCUSSION

Basic FeP Synthesis Procedure

A basic FeP synthesis procedure was developed based on literature reports by Schaak and co-workers.[38,43] A number of parameters were evaluated to optimize the formation of phase pure FeP particles. The evaluation process is described in the following sections. In the basic procedure, nanobundles of FeP were prepared through the reaction of presynthesized β-FeOOH nanoneedles with TOP, which acted as the phosphorus source, the stabilizing ligand, and the solvent at elevated temperatures. This process is illustrated in Scheme 1. The needle-shaped β-FeOOH nanostructures were synthesized by the hydrolysis of 20 mmol $FeCl_3{\cdot}6H_2O$ in the presence of poly(ethyleneimine) (PEI, MW = 750,000) as described previously.[44−46] The β-FeOOH powder was heated with 5.38 mmol of TOP at 320 °C under an argon atmosphere. The basic Fe_xP nanoparticle synthesis was performed using 0.66 mmol (0.059 g) of β-FeOOH powder and heated with 5.38 mmol of TOP at 320 °C under an argon atmosphere. See Table S1 for the various reaction conditions.

It took 70 min to reach 320 °C from room temperature, and the color of the reaction mixture changed from yellowish-brown to black above 200 °C. The solution was aged at 320 °C for 4.5 h and subsequently cooled to room temperature. The black product was precipitated by adding an excess of ethanol (5−10 mL). The black particles were isolated by centrifugation and dried in a vacuum desiccator overnight. Figure 1a−c displays the transmission electron microscopy (TEM) images of the iron phosphide nanoparticles that were synthesized using 5.38 mmol of TOP at 320 °C for 4.5 hours. The images show a drastic change in the morphology of nanoparticles from nanoneedles ($l \sim 90$ nm, $w \sim 12$ nm) to nanobundles. The typical dimensions of individual rods/branches of a nanobundle ranged from 500 nm to 1 μm (Figure 1b). Figure 1c shows a high-resolution TEM (HRTEM) image of the lattice fringes of a nanobundle branch. A d-spacing of 0.29 nm corresponds to the (020) plane of FeP. The pXRD pattern of

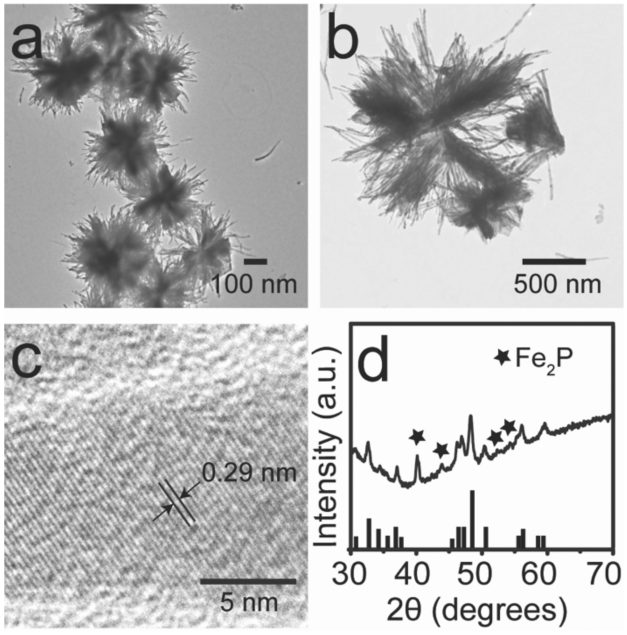

Figure 1. (a, b) TEM images of Fe_xP nanobundles synthesized using the basic procedure. (c) HRTEM image of a nanobundle branch. The lattice spacing (d_{020} = 0.29 nm) corresponds to the FeP phase. (d) Representative pXRD pattern of the mixture of Fe_xP phases that results from the basic synthesis procedure. The tick marks represent the reference pattern for FeP (JCPD 01-071-2262), and Fe_2P is indicated with stars (JCPD 01-051-0943).

https://doi.org/10.1021/acsnanoscienceau.3c00036
ACS Nanosci. Au 2023, 3, 491−499

Fe_xP nanobundles reveals the formation of two crystalline phases that can be indexed to FeP with space group $Pna2_1$ (JCPD 01-071-2262) and Fe_2P with space group $P\bar{6}2m$ (JCPD 01-051-0943). The intense peaks at ∼40° and 44° were assigned to the (111) and (201) planes, respectively, of the minor product, Fe_2P.

In Figure 2a, the high-resolution Fe 2p core level spectrum of Fe_xP nanobundles from X-ray photoelectron spectroscopy

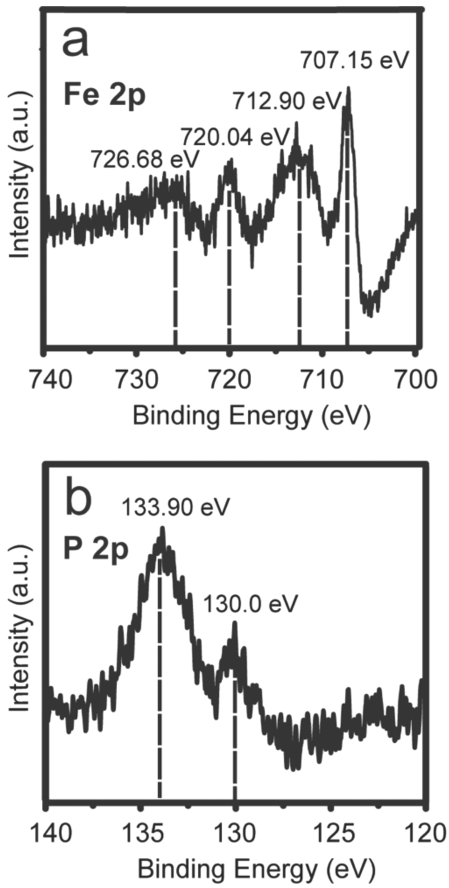

Figure 2. XPS core level spectra of Fe_xP nanobundle samples generated using the basic synthesis procedure: (a) Fe 2p region and (b) P 2p region.

(XPS) displays four peaks. Two peaks at binding energies (BEs) of 712.90 eV (Fe $2p_{3/2}$) and 726.68 eV (Fe $2p_{1/2}$) are associated with Fe^{3+} from iron oxide and iron phosphate due to sample oxidation from air exposure. The other two peaks at BEs of 707.15 and 720.04 eV are ascribed to Fe^{3+} from FeP.[5,20,42,45,47] Furthermore, in Figure 2b, the P 2p core-level XPS spectrum shows two peaks at BEs of 130.0 and 133.9 eV; these peaks, respectively, correspond to the phosphorus anion of iron phosphide and an oxidized iron-phosphate species like PO_4^{3-} or P_2O_5, resulting from surface oxidation.[5,42,48,49]

Our basic synthesis resulted in a nanobundle morphology with a mixture of both FeP and Fe_2P phases. A series of reactions were performed to determine the optimal reaction conditions to generate phase pure FeP nanobundles such as varying the amount of phosphorus precursor (TOP), the reaction time, and heating rate (°C/min), which are described in subsequent sections.

Reaction Series I: Effect of Trioctylphosphine

We explored a series of reactions to determine how the amount of TOP affected the phase purity of the resulting FeP nanoparticles. TOP is simultaneously the phosphorus source, solvent, and surfactant/stabilizer in this reaction.[6,8,39,50] At high temperatures (ranging from 290 to 370 °C), the breakdown of the P−C bond in TOP generates less active phosphorus species compared with the breakdown of the P−Si bond in $P(SiMe_3)_3$, a compound used in other TMP synthesis protocols. Generally, $P(SiMe_3)_3$ is used as a stoichiometric reagent, whereas TOP is used in excess.[27,51] This disparity may be attributed to the bond energy required to break the P−C bonds, which requires elevated temperatures, hinders efficient phosphorus activation and reduces the availability of active phosphorus to react with the iron precursor.[12,39,50]

In Reaction Series I, the amount of TOP was varied from 3.96 to 16.6 mmol with the intent of increasing the amount of active phosphorus available to react with β-FeOOH to produce phase pure FeP. All other parameters were kept constant: the amount of β-FeOOH (0.66 mmol, 0.059 g), temperature (320 °C), heating rate (4.5 °C/min), and heating time (4.5 h). The mole ratio of the Fe precursor to TOP varied from 1:6 to 1:25. The number of moles of β-FeOOH was determined by deducting the mass of the ligand (PEI) from the total mass. The microstructure of Fe_xP nanocrystalline products was investigated by TEM. In general, the morphologies of the nanoparticle samples in Reaction Series I were comparable and varied from nanorods to nanobundles, with the major distinguishing factor being the texture and crystallinity. For the sample containing 3.96 mmol of TOP, the morphology consisted of individual rods with lengths ranging between 700 nm and 2 μm (Figure 3a). The inset in Figure 3b shows a

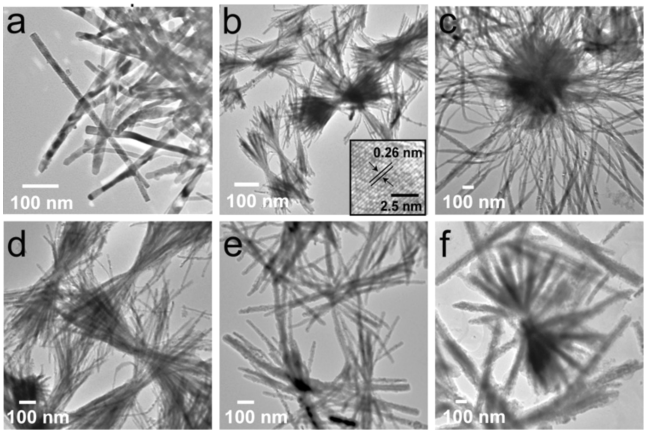

Figure 3. Reaction Series I. TEM images of Fe_xP nanoparticles synthesized with varying amounts of TOP: (a) 3.96, (b) 4.64, (c) 5.96, (d) 6.72, (e) 9.96, and (f) 16.6 mmol. HRTEM images of lattice fringes of FeP particles with d_{200} = 0.26 nm (inset in (b)).

HRTEM image with well-resolved lattice fringes with interplanar spacing d_{200} = 0.26 nm of FeP (JCPD 01-071-2262, space group $Pna2_1$). Furthermore, Figure 3b−f illustrates that the level of roughness/texture of the nanobundles increased with the amount of TOP.

Figure 4 shows pXRD patterns for Reaction Series I. Larger β-FeOOH:TOP millimole ratios typically result in a mixture of the two phases: FeP and Fe_2P. The crystallinity of the Fe_2P phase improved with a 1:15 mmol ratio of β-FeOOH:TOP, as

https://doi.org/10.1021/acsnanoscienceau.3c00036
ACS Nanosci. Au 2023, 3, 491−499

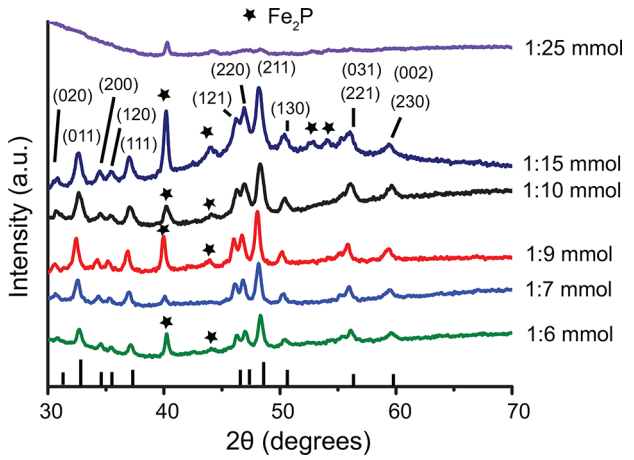

Figure 4. Reaction Series I. PXRD patterns of the Fe_xP samples as a function of the β-FeOOH:TOP mmol ratio. The reactions were performed at 320 °C for 4.5 h. The reference pXRD pattern of FeP is represented by black tick marks, and that of Fe_2P with stars.

indicated by the presence of additional reflections and the sharp diffraction peak at 40° that corresponds to the (111) planes of Fe_2P. In order to shift the reaction towards the production of the Fe_2P phase, the β-FeOOH:TOP ratio was increased to 1:25 mmol. The sample had fewer reflections and was less crystalline, but intense peaks were attributed to the Fe_2P phase. Moreover, pXRD results were consistent with TEM image analysis, revealing that the surface of bundles was rough, the particles were porous, and the grain sizes were smaller when compared to samples with lower amounts of TOP (Figure 3a–f). Nonetheless, the persistence of the two phases across Reaction Series I indicated that this strategy was inconsistent with the goal of obtaining phase pure FeP. While the Fe_2P phase appears to be favored at higher concentrations of TOP, we did not investigate the optimization of this phase further. Sun et al. also observed Fe_2P as the major product with greater amounts of the phosphorus source. This is because Fe_2P is favored at lower temperatures and at a lower atomic percent of phosphorus, which is consistent with the Fe–P binary phase diagram.

Reaction Series II: Effect of Reaction Time

Next, we explored the role of the reaction time on the phase purity of FeP nanoparticles. We presumed that the longer reaction time would lead to a higher availability of active phosphorus to react β-FeOOH. We varied the reaction time from 1 to 12 h and kept the amount of β-FeOOH (0.66 mmol, 0.059 g), temperature (320 °C), amount of TOP (3.96 mmol), and heating rate (4.5 °C/min) constant. TEM images of the resultant products are presented in Figure 5. After reacting for one hour, neither the nanoneedle morphology nor the size of the β-FeOOH precursor was maintained (Figure 5a). The dimensions of the β-FeOOH were l = 90 ± 15 nm and w = 12 ± 4 nm prior to reacting with TOP. In Figure 5a, the black arrow indicates the presence of porous nanorods (lighter contrast region). It is possible that these structures were formed due to the exoteric diffusion of iron ions from the surface.[41,52,53] The products synthesized at longer times (4 h and 6 h) formed longer rods and bundles as shown in Figure 5b and c. After 12 h, the nanobundles began to separate into individual rods, possibly breaking down from the center, as shown in Figure 5d. Additionally, the rough/undulated surface

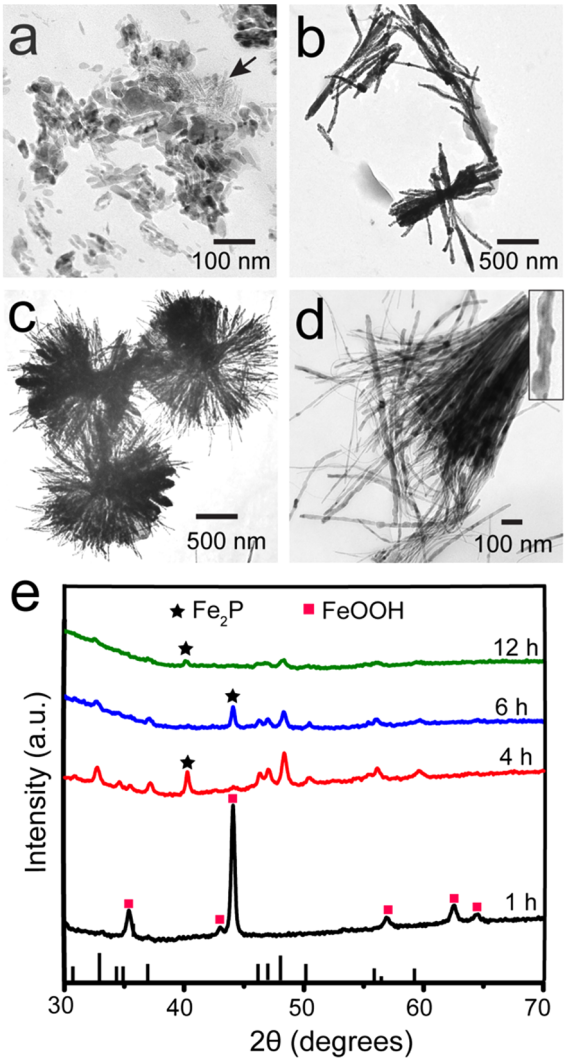

Figure 5. Reaction Series II. TEM images of nanoparticle products synthesized as a function of reaction time: (a) 1, (b) 4, (c) 6, and (d) 12 h. The black arrow in panel (a) emphasizes lighter contrast regions due to porous particles. (e) PXRD patterns for time series experiments (a)–(d). Black tick marks and red squares indicate the reference pXRD patterns for FeP and β-FeOOH, respectively. The reflections attributed to Fe_2P are highlighted with stars.

of nanostructures was observed at longer reaction times, as evidenced by TEM (inset of Figure 5d).

Figure 5e shows the pXRD patterns of the samples from Reaction Series II. At 1 h, the reaction mixture changed from brownish-yellow to black. The pXRD peaks for the 1 h sample corresponded to β-FeOOH (JCPD 00-34-1266) with a slight shift from the standard pattern. This may be due to the diffusion of reactive phosphorus species into the β-FeOOH crystal lattice. Characteristic diffraction peaks at 2θ = 32.7°, 34.5°, 35.4°, 37.1°, 46.3°, 47.0°, 48.3°, 50.4°, 56.1°, and 59.6° corresponding to (011), (200), (120), (111), (121), (220), (211), (130), (221), and (002) of FeP (JCPD -1-071-2262) and (111) at 40.3° of Fe_2P (JCPD 00-051-0943) appeared after 4 h of heating. This confirms the complete phase transformation of β-FeOOH to mixed phases of iron phosphide (FeP and Fe_2P). Heating the Fe_xP nanobundles for 6 h did not increase the purity of the phase. Moreover, when heated for 12 h, the material lost its crystalline structure.

https://doi.org/10.1021/acsnanoscienceau.3c00036
ACS Nanosci. Au 2023, 3, 491–499

Reaction Series III, IV, and V: Effect of Injecting Preheated TOP, Temperature, and Amount of β-FeOOH

In Reaction Series III, IV, and IV, we explored the impact of injecting preheated TOP, increasing the reaction temperature, and adjusting the amount of β-FeOOH to obtain pure FeP nanoparticles. The data for these experiments is shown in Figure 6. In all of the strategies discussed earlier, TOP was

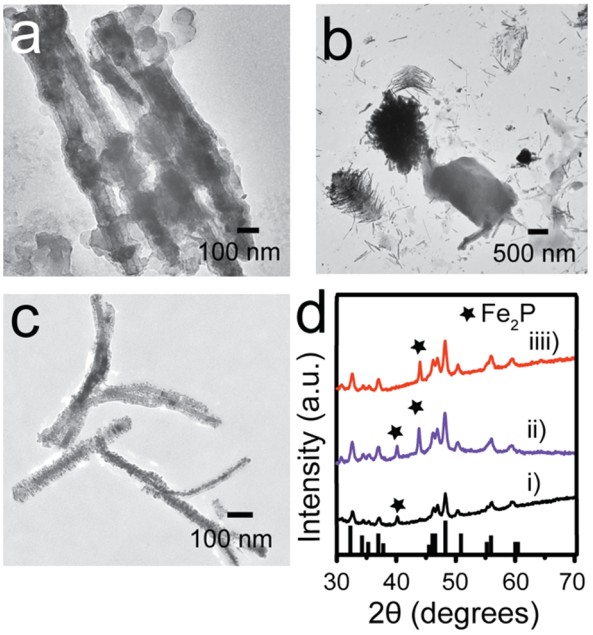

Figure 6. TEM images of Fe_xP particles under different reaction conditions: (a) hot injection of TOP, (b) heating at 350 °C, and (c) increased amount of iron β-FeOOH. (d) PXRD patterns of samples synthesized by (i) hot injection of TOP, (ii) heating at 350 °C, and (iii) an increased amount of iron β-FeOOH. PXRD patterns for FeP (black tick marks) and Fe_2P (stars) are shown for reference.

added to β-FeOOH at room temperature. In Reaction Series III, we hypothesized that the addition of preheated TOP could release more reactive phosphorus species that could drive the complete transformation of the precursors to phase pure FeP. In order to test this presumption, we decided to inject the hot (100 °C) TOP solution into the reaction mixture of β-FeOOH with TOP stirring at 320 °C. After hot injection, the reaction mixture was aged at 320 °C for 4.5 h. The image of the final product obtained from TEM showed that elongated and irregular nanostructures were formed, as seen in Figure 6a. In Reaction Series IV, we evaluated whether a higher temperature could promote the formation of single-phase FeP since increasing the temperature can speed up the diffusion rate of phosphorus, as previously reported in the literature.[52,54] The experiment was conducted using the same conditions with 0.66 mmol of β-FeOOH and 3.96 mmol of TOP, but with a temperature change to 350 °C. The TEM image in Figure 6b illustrates the development of fernlike fractal structures in conjunction with some individual nanorods. Unlike other literature reports, a larger amount of TOP and a higher temperature did not favor the formation of the phosphorus-rich FeP.[8] In Reaction Series IV, we increased the amount of β-FeOOH from 0.66 mmol (0.059 g) to 1.0 mmol (0.089 g) while keeping all of the other reaction parameters constant. Figure 6c shows a TEM image of this sample, indicating the formation of dendritic, rod-like (l = 300 − 600 nm) nanostructures. Despite the differences in the shape of the resultant particles in Reaction Series III and IV, pXRD patterns shown in Figure 6d confirmed that the products consist of a mixture of both FeP and Fe_2P phases. The intensity of some of the reflections of the Fe_2P phase is affected likely as a result of the morphologies of the particles. Taken together, the results indicate that phase control of FeP was not achieved under the conditions evaluated in this series of reactions that included the hot injection of TOP, increasing the temperature, and adjusting the amount of β-FeOOH.

Reaction Series VI: Effect of the Heating Rate (°C/min)

In Reaction Series VI, the heating rate was increased to 18.8 °C/min to reach the target temperature of 320 °C and maintained for a variable period. We were inspired by Sun group who reported that heating rate played a role in generating phase pure iron phosphide materials.[5] All other parameters were maintained at 0.66 mmol of β-FeOOH and 3.96 mmol of TOP, as shown in Table S2. Figure 7 shows the

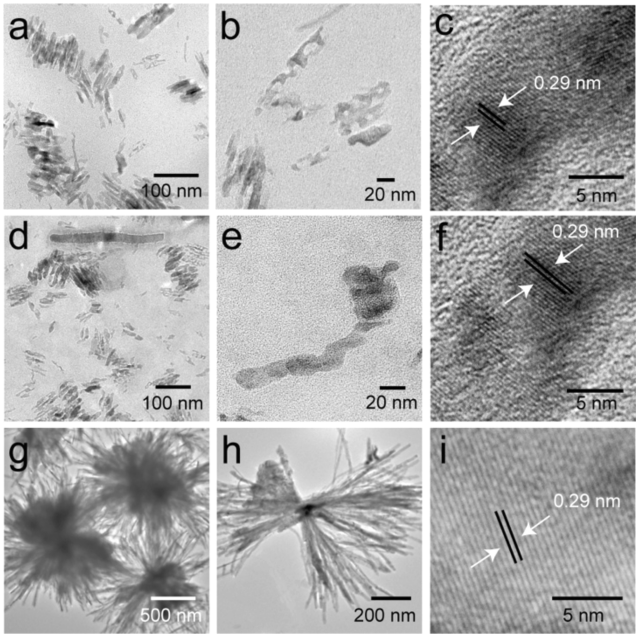

Figure 7. TEM images of Fe_xP nanoparticles with respect to reaction time (a−c) 1 h, (d−f) 2 h, and (g−i) 4.5 h at a heat rate of 18.8 °C/min. The lattice spacing (d_{020} = 0.29 nm) corresponds to the FeP phase, which is present in small amounts in the 1 and 2 h samples.

changes in the morphology of the particles throughout the reaction. Porous particles are observed within 1−2 h of reaction time (Figure 7a−f). The sizes of porous structures range from 50 to 70 nm after 1 h of heating. This is a significant change in the original morphology and size ranges of the β-FeOOH nanoneedles. These hollow-porous structures may be due to the inward diffusion of phosphorus and the outward diffusion of iron, analogous to the Kirkendall effect.[41,52] However, the dehydration of the β-FeOOH nanoneedles under high temperatures could also lead to the formation of pores.[41,46] On heating for 4.5 h, the rod-shaped particles arranged into nanobundles (Figure 7g and h). Individual rods making up the bundle were ∼800−1400 nm in length and ∼18 nm in width. A HRTEM image of the particles at a reaction time of 4.5 h reveals lattice fringes with a d-spacing of 0.29 nm, corresponding to the (020) plane of the

https://doi.org/10.1021/acsnanoscienceau.3c00036
ACS Nanosci. Au 2023, 3, 491−499

FeP phase (Figure 7i). Figure 8a displays pXRD patterns, which indicate that the products produced at shorter reaction

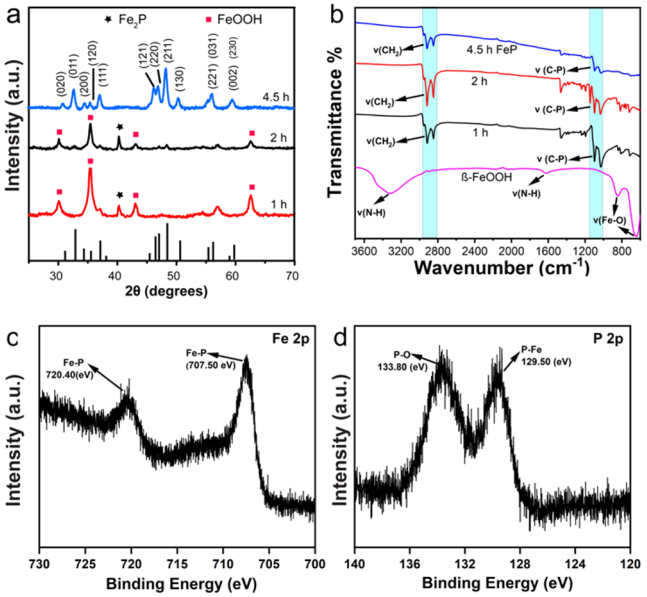

Figure 8. Reaction Series VI. Characterization of Fe_xP nanoparticle samples from synthetic experiments with a fast heating rate (18.8 °C/min): (a) pXRD patterns and (b) FTIR spectra of the samples as a function of reaction time. High-resolution XPS core level spectra of the Fe 2p (c) and P 2p (d) regions of the phase pure FeP nanoparticles synthesized at a heating rate of 18.8 °C/min for 4.5 h.

times (1 and 2 h) comprise mostly of β-FeOOH, small amounts of FeP, and some Fe_2P, as evidenced by the peak at 40.3°. However, a longer heating time (4.5 h) results in the formation of phase pure FeP. No other phases of iron phosphide, including Fe_2P, were detected in the pattern. Energy dispersive X-ray spectroscopy shows an elemental composition of approximately 1:1 atom % Fe:P (Figure S1).

FeP nanobundles were further characterized by FTIR and XPS. Figure 8b shows the FTIR spectra with distinct absorption bands consistent with TOP at ∼ 2800−3000 and 1100−1200 cm^{-1} corresponding to −C−H stretching and −C−P stretching, respectively.[55] All the samples evaluated in the time series (1, 2, and 4.5 h) showed the same signature peaks for TOP (Table S2). This observation suggests TOP coordinates with the surface of the particles and serves as a capping agent. This also suggests that there is only partial breaking of the P−C bond of TOP at all time points. This could be caused by the relatively high energy needed to break the P−C bonds.[6,31] Quick heating rates could help activate the P−C bond of TOP and generate more reactive phosphorus species to react with β-FeOOH to form FeP.[31,50] Figure 8c and d represents the high-resolution XPS core level spectra of the Fe 2p and P 2p regions, respectively, of the phase pure FeP nanoparticles synthesized at 4.5 h. The peaks assigned to Fe $2p_{3/2}$ and Fe $2p_{1/2}$ centered at 707.5 and 720.4 eV, respectively, are in good agreement with the BE values for phase pure FeP reported in the literature.[18,30] The high-resolution P 2p spectrum exhibited peaks at 129.5 eV corresponding to the P^{3-} anion ($2p_{3/2}$) and another one at 133.8 eV, attributed to an oxidized phosphorus species.[18,42,48] The peak at a BE of 129.5 eV (P $2p_{3/2}$) is characteristic of the FeP phase. These results are consistent with and support previous reports in the literature.[18,42]

CONCLUSION

We report a wet chemical approach to synthesize phase pure iron phosphide FeP nanobundles using β-FeOOH as an iron precursor and TOP as a phosphorus source under mild conditions. Several reaction parameters such as reaction time, temperature, precursor concentration, and heating rate were varied to understand their effect on the morphology and phase of the resulting product. The investigation confirms that the conversion of β-FeOOH into FeP is dependent on the heating rate (18.8 °C/min) when TOP is the phosphorous source. At a slower heat rate (4.5 °C/min), transformation to FeP is incomplete, suggesting the presence of a kinetic barrier (likely the formation of Fe_2P). The formation of FeP may occur through in situ transformation of the Fe_2P phase where a fast heating rate likely shifts the equilibrium in favor of FeP. The observed partial completion of the reaction could be caused by the lower availability of active phosphorus, which is a consequence of the incomplete breaking of the phosphorus-carbon (P−C) bond within tri-n-octylphosphine (TOP), as well as the sluggish mobility of the active phosphorus species. The faster heating rate (18.8 °C/min) alleviates the mobility and the concentration issues of an active phosphorous species which facilitates reaction with the β-FeOOH nanoneedles.

METHODS

Materials

Ferric chloride hexahydrate ($FeCl_3{\cdot}6H_2O$, 98% ACS grade), a 50% (w/v) poly(ethyleneimine) solution (PEI, MW 750,000), and tri-*n*-octylphosphine (TOP, $P(C_8H_{17})_3$, ≥90% technical grade) were purchased from Sigma-Aldrich (St. Louis, MO). Anhydrous ethyl alcohol 200 proof (absolute, ACS/USP grade) and hexane (ACS/USP grade) were purchased from Pharmco (Brookfield, CT). Transmission electron microscopy (TEM) Cu grids (carbon-coated, 200 mesh) were purchased from Electron Microscopy Sciences (Hatfield, PA).

Preparation of Iron Oxyhydroxide (β-FeOOH) Nanoneedles

Iron oxyhydroxide nanoneedles were prepared using a simple hydrolysis method reported in the literature with some minor modifications.[42−44] Typically, 5.4 g (20.0 mmol) of solid $FeCl_3{\cdot}6H_2O$ was dissolved in 100 mL of DI water (18.2 Ω/cm) at room temperature in a 500 mL three-necked round-bottomed flask fitted with a condenser. Next, 621 μL of a 47.5% v/v PEI solution was added in a dropwise manner to the reaction mixture with stirring (400 rpm). The reaction was maintained at 80 °C in an oil bath for 2 h. Finally, the brownish-yellow precipitate was collected by high-speed centrifugation at 8000 rpm for 15 min, washed several times with ethanol, and dried in a vacuum desiccator (Nalgene) overnight. The dimensions of the β-FeOOH nanoneedles were approximately l = 90 ± 15 nm and w = 12 ± 4 nm as measured from TEM images using Image J (version: 1.54d) software.

Preparation of FeP Nanobundles

The reaction was carried out under an inert atmosphere (Ar). Argon gas was purged for 30 min to remove oxygen from the round bottom flask. Typically, the synthesis involves two steps: (i) synthesis of β-FeOOH nanoneedles and (ii) successive conversion of β-FeOOH nanoneedles to FeP by treatment with TOP. A reaction mixture of 0.059 g of β-FeOOH with 3.96 mmol of TOP was heated at a rate of 18.8 °C/min to reach 320 °C within 17 min from room temperature. The temperature was allowed to quickly climb to 340 °C where the reaction mixture was aged for 10 min. Afterward, the reaction mixture

https://doi.org/10.1021/acsnanoscienceau.3c00036
ACS Nanosci. Au 2023, 3, 491−499

was cooled to 320 °C and maintained at this temperature for 4.5 h under an argon atmosphere with continuous stirring (600 rpm). After cooling the system to room temperature, the final product was isolated by adding excess ethanol (10−20 mL) and centrifuging at 8,000 rpm for 2 min in an Eppendorf tube to isolate the solid particles. The black solid was washed several times with hexanes, until the supernatant was clear. The FeP particles were dried in a vacuum desiccator (Nalgene) overnight. See Table S1 for variations on the synthesis protocol.

Characterization Techniques

The morphology and size of the resulting nanoparticles were determined with a JEOL JEM 2100 transmission electron microscope (TEM) at an accelerating voltage of 200 kV and a beam current of 102 μA. Powder X-ray diffraction (pXRD) patterns of the resulting product were acquired by a Rigaku Smart Lab X-ray Diffractometer with a Cu Kα radiation source (λ = 1.54 Å). The 2θ scan range was varied from 5° to 90° at a scan rate of 5°/min. X-ray photoelectron spectroscopy (XPS) was conducted with a base pressure of less than 10^{-10} Torr at ambient temperature. The spectra were obtained by using the Al Kα emission line from a dual-anode X-ray source (PREVAC XR 40B) operated at 405 W with an incident angle of 54.7° and normal emission. The kinetic energy of the photoelectrons was collected and analyzed with an EA 125-hemispherical electron energy analyzer with a resolution of 0.025 eV. FTIR instrument spectra were recorded on a Thermo Scientific Nicolet instrument.

■ ASSOCIATED CONTENT

Supporting Information

The Supporting Information is available free of charge at https://pubs.acs.org/doi/10.1021/acsnanoscienceau.3c00036.

Table containing reaction parameters for the synthesis of FeP; table of products produced at various times at a heat rate of 18.8 °C/min; and EDS data of FeP nanobundles (PDF)

■ AUTHOR INFORMATION

Corresponding Author

Yolanda Vasquez − *Department of Chemistry, Oklahoma State University, Stillwater, Oklahoma 74078, United States;* orcid.org/0000-0002-3991-5975; Email: yolanda.vasquez@okstate.edu

Authors

Menuka Adhikari − *Department of Chemistry, Oklahoma State University, Stillwater, Oklahoma 74078, United States;* Present Address: Department of Chemistry, Physics and Materials Sciences, Fayetteville State University, Fayetteville, NC 28301, United States

Shubham Sharma − *Department of Chemistry, Oklahoma State University, Stillwater, Oklahoma 74078, United States*

Elena Echeverria − *Department of Physics, Oklahoma State University, Stillwater, Oklahoma 74078, United States;* orcid.org/0000-0002-9472-6288

David N. McIlroy − *Department of Physics, Oklahoma State University, Stillwater, Oklahoma 74078, United States;* orcid.org/0000-0001-9438-3775

Complete contact information is available at: https://pubs.acs.org/10.1021/acsnanoscienceau.3c00036

Author Contributions

†M.A. and S.S. contributed equally. M.A. and Y.V. designed the project. S.S., M.A., and Y.V. wrote the manuscript. M.A. and S.S. performed the synthetic and materials characterization experiments. S.S., M.A., and Y.V. analyzed the data. E.E. and D.N.M performed XPS experiments and analyzed the data. All authors have given approval to the final version of the manuscript. CRediT: **Menuka Adhikari** conceptualization, data curation, formal analysis, investigation, writing-original draft; **Shubham Sharma** data curation, formal analysis, investigation, writing original draft, writing-review & editing; **Elena Echeverria** data curation, formal analysis; **David N. McIlroy** data curation, formal analysis, resources; **Yolanda Vasquez** conceptualization, data curation, formal analysis, funding acquisition, project administration, resources, supervision, writing-review & editing.

Funding

This work was supported by the National Science Foundation (United States) CAREER Award (CHE 1554924).

Notes

The authors declare no competing financial interest.

■ ACKNOWLEDGMENTS

M.A., S.S., and Y.V. would like to thank Lisa Whitworth and Brent Johnson at the OSU Microscopy Lab (Stillwater, OK) for their assistance with XRD and TEM.

■ ABBREVIATIONS

TOP, tri-*n*-octylphosphine; TOPO, trioctylphosphine oxide; PEI, poly(ethyleneimine)

■ REFERENCES

(1) Yuan, H.; Chen, X.; Zhou, G.; Zhang, W.; Luo, J.; Huang, H.; Gan, Y.; Liang, C.; Xia, Y.; Zhang, J.; Wang, J.; Tao, X. Efficient Activation of Li_2S by Transition Metal Phosphides Nanoparticles for Highly Stable Lithium−Sulfur Batteries. *ACS Energy Lett.* **2017**, *2* (7), 1711−1719.

(2) Stutz, E. Z.; Zamani, M.; Damry, D. A.; Buswell, L.; Paul, R.; Escobar Steinvall, S.; Leran, J.-B.; Boland, J. L.; Dimitrievska, M.; Fontcubertai Morral, A. Showcasing the Optical Properties of Monocrystalline Zinc Phosphide Thin Films as an Earth-Abundant Photovoltaic Absorber. *Mater. Adv.* **2022**, *3* (2), 1295−1303.

(3) Zhang, N.; Li, Y.; Xu, J.; Li, J.; Wei, B.; Ding, Y.; Amorim, I.; Thomas, R.; Thalluri, S. M.; Liu, Y.; Yu, G.; Liu, L. High-Performance Flexible Solid-State Asymmetric Supercapacitors Based on Bimetallic Transition Metal Phosphide Nanocrystals. *ACS Nano* **2019**, *13* (9), 10612−10621.

(4) Brock, S. L.; Senevirathne, K. Recent Developments in Synthetic Approaches to Transition Metal Phosphide Nanoparticles for Magnetic and Catalytic Applications. J. *Solid State Chem.* **2008**, *181* (7), 1552−1559.

(5) Wang, J.; Yang, Q.; Zhang, Z.; Sun, S. Phase-Controlled Synthesis of Transition-Metal Phosphide Nanowires by Ullmann-Type Reactions. *Eur. J. Chem.* **2010**, *16*, 7916−7924.

(6) Chiang, R-K.; Chiang, R-T. Formation of Hollow Ni_2P Nanoparticles Based on the Nanoscale Kirkendall Effect. *Inorg. Chem.* **2007**, *46*, 369−371.

(7) Park, J.; Koo, B.; Yoon, Y. K.; Hwang, Y.; Kang, M.; Park, J-G.; Hyeon, T. Generalized Synthesis of Metal Phosphide Nanorods via Thermal Decomposition of Continuously Delivered Metal−Phosphine Complexes Using a Syringe Pump. *J. Am. Chem. Soc.* **2005**, *127*, 8433−8440.

(8) Gregg, K. A.; Perera, S. C.; Lawes, G.; Shinozaki, S.; Brock, S. L. Controlled Synthesis of MnP Nanorods: Effect of Shape Anisotropy on Magnetization. *Chem. Mater.* **2006**, *18*, 879−886.

(9) Popczun, E. J.; McKone, J. R.; Read, C. G.; Biacchi, A. J.; Wiltrout, A. M.; Lewis, N. S.; Schaak, R. E. Nanostructured Nickel Phosphide as an Electrocatalyst for the Hydrogen Evolution Reaction. *J. Am. Chem. Soc.* **2013**, *135*, 9267−9270.

(10) Blanchard, P. E. R.; Grosvenor, A. P.; Cavell, R. G.; Mar, A. X-Ray Photoelectron and Absorption Spectroscopy of Metal-Rich Phosphides M_2P and M_3P (M = Cr−Ni). *Chem. Mater.* **2008**, *20*, 7081−7088.
(11) Brock, S. L.; Perera, S. C.; Stamm, K. L. Chemical Routes for Production of Transition-Metal Phosphides on the Nanoscale: Implications for Advanced Magnetic and Catalytic Materials. *Eur. J. Chem.* **2004**, *10*, 3364−3371.
(12) Muthuswamy, E.; Kharel, R. P.; Lawes, G.; Brock, S. L. Control of Phase in Phosphide Nanoparticles Produced by Metal Nanoparticle Transformation: Fe_2P and FeP. *ACS Nano* **2009**, *3*, 2383−2393.
(13) Xu, Y.; Wu, R.; Zhang, J.; Shi, Y.; Zhang, B. Anion-Exchange Synthesis of Nanoporous FeP Nanosheets as Electrocatalysts for Hydrogen Evolution Reaction. *Chem. Comm.* **2013**, *49*, 6656−6658.
(14) Schipper, D. E.; Zhao, Z.; Thirumalai, H.; Leitner, A. P.; Donaldson, S. L.; Kumar, A.; Qin, F.; Wang, Z.; Grabow, L. C.; Bao, J.; Whitmire, K. H. Effects of Catalyst Phase on the Hydrogen Evolution Reaction of Water Splitting: Preparation of Phase-Pure Films of FeP, Fe_2P, and Fe_3P and Their Relative Catalytic Activities. *Chem. Mater.* **2018**, *30*, 3588−3598.
(15) Du, Y.; Yue, G.; Lan, Z.; Gao, Y.; Wu, J.; Tan, F. A Dye-Sensitized Solar Cell Based on Magnetic CoP@FeP_4@Carbon Composite Counter Electrode Generated an Efficiency of 9.88%. Inorg. *Chem. Front.* **2021**, *8*, 5034−5044.
(16) Chen, Y.; Li, T.; Zhao, Q.; Liu, D.; Li, C.- M. The in-Situ Preparation of Iron Phosphide Using Ionic Liquids as Iron and Phosphorus Sources for Efficient Hydrogen Evolution Reactions. *RSC Adv.* **2020**, *10*, 33026−33032.
(17) Yao, S.; Forstner, V.; Menezes, P. W.; Panda, C.; Mebs, S.; Zolnhofer, E. M.; Miehlich, M. E.; Szilvási, T.; Ashok Kumar, N.; Haumann, M.; Meyer, K.; Grützmacher, H.; Driess, M. From an Fe_2P_3 Complex to FeP Nanoparticles as Efficient Electrocatalysts for Water-Splitting. *Chem. Sci.* **2018**, *9*, 8590−8597.
(18) Liang, Y.; Liu, Q.; Asiri, A. M.; Sun, X.; Luo, Y. Self-Supported FeP Nanorod Arrays: A Cost-Effective 3D Hydrogen Evolution Cathode with High Catalytic Activity. *ACS Catal.* **2014**, *4* (11), 4065−4069.
(19) Ma, F.-X.; Xu, C.-Y.; Lyu, F.; Song, B.; Sun, S.-C.; Li, Y. Y.; Lu, J.; Zhen, L. Construction of FeP Hollow Nanoparticles Densely Encapsulated in Carbon Nanosheet Frameworks for Efficient and Durable Electrocatalytic Hydrogen Production. *Adv. Sci.* **2019**, *6*, No. 1801490.
(20) Tian, L.; Yan, X.; Chen, X. Electrochemical Activity of Iron Phosphide Nanoparticles in Hydrogen Evolution Reaction. *ACS Catal.* **2016**, *6*, 5441−5448.
(21) Wang, C.; Yan, J.; Li, T.; Lv, Z.; Hou, X.; Tang, Y.; Zhang, H.; Zheng, Q.; Li, X. A Coral-Like FeP@NC Anode with Increasing Cycle Capacity for Sodium-Ion and Lithium-Ion Batteries Induced by Particle Refinement. *Angew. Chem. Int. Ed.* **2021**, *60*, 25013−25019.
(22) Wang, X.; Chen, K.; Wang, G.; Liu, X.; Wang, H. Rational Design of Three-Dimensional Graphene Encapsulated with Hollow FeP@Carbon Nanocomposite as Outstanding Anode Material for Lithium Ion and Sodium Ion Batteries. *ACS Nano* **2017**, *11*, 11602−11616.
(23) Zhu, P.; Zhang, Z.; Hao, S.; Zhang, B.; Zhao, P.; Yu, J.; Cai, J.; Huang, Y.; Yang, Z. Multi-Channel FeP@C Octahedra Anchored on Reduced Graphene Oxide Nanosheet with Efficient Performance for Lithium-Ion Batteries. *Carbon* **2018**, *139*, 477−485.
(24) Zhang, X.; Yang, W. O.; Zhu, G.; Lu, T.; Pan, L. Shuttle-like Carbon-Coated FeP Derived from Metal-Organic Frameworks for Lithium-Ion Batteries with Superior Rate Capability and Long-Life Cycling Performance. *Carbon* **2019**, *143*, 116−124.
(25) Li, X.; Wang, X.; Yang, W.; Zhu, Z.; Zhao, R.; Li, Q.; Li, H.; Xu, J.; Zhao, G.; Li, H.; Li, S. Three-Dimensional Hierarchical Flowerlike FeP Wrapped with N-Doped Carbon Possessing Improved Li+ Diffusion Kinetics and Cyclability for Lithium-Ion Batteries. *ACS Appl. Mater. Interfaces* **2019**, *11*, 39961−39969.
(26) Stamm, K. L.; Garno, J. C.; Liu, G. -Y.; Brock, S. L. A General Methodology for the Synthesis of Transition Metal Pnictide Nanoparticles from Pnictate Precursors and Its Application to Iron−Phosphorus Phases. *J. Am. Chem. Soc.* **2003**, *125*, 4038−4039.
(27) Perera, S. C.; Fodor, P. S.; Tsoi, G. M.; Wenger, L. E.; Brock, S. L. Application of De-Silylation Strategies to the Preparation of Transition Metal Pnictide Nanocrystals: The Case of FeP. *Chem. Mater.* **2003**, *15*, 4034−4038.
(28) Park, J.; Koo, B.; Hwang, Y.; Bae, C.; An, K.; Park, J.-G.; Park, H.M.; Hyeon, T. Novel Synthesis of Magnetic Fe_2P Nanorods from Thermal Decomposition of Continuously Delivered Precursors Using a Syringe Pump. *Angew. Chem. Int. Ed.* **2004**, *43*, 2282−2285.
(29) Luo, F.; Su, H.; Song, W.; Wang, Z.; Yan, Z.; Yan, C. Magnetic and Magnetotransport Properties of Fe_2P Nanocrystallites via a Solvothermal Route. *J. Mater. Chem.* **2004**, *14*, 111−115.
(30) Li, Y.; Malik, M. A.; O'Brien, P. Synthesis of Single-Crystalline CoP Nanowires by a One-Pot Metal−Organic Route. *J. Am. Chem. Soc.* **2005**, *127*, 16020−16021.
(31) Chen, J.; Tai, M.; Chi, K. Catalytic Synthesis, Characterization and Magnetic Properties of Iron Phosphide Nanowires. *J. Mater. Chem.* **2004**, *14*, 296−298.
(32) Kelly, A. T.; Rusakova, I.; Ould-Ely, T.; Hofmann, C.; Lüttge, A.; Whitmire, K. H. Iron Phosphide Nanostructures Produced from a Single-Source Organometallic Precursor: Nanorods, Bundles, Crosses, and Spherulites. *Nano Lett.* **2007**, *7*, 2920−2925.
(33) Hu, X.; Yu, C. J. High-Yield Synthesis of Nickel and Nickel Phosphide Nanowires via Microwave-Assisted Processes. *Chem. Mater.* **2008**, *20*, 6743−6749.
(34) Barry, B. M.; Gillan, E. G. Low-Temperature Solvothermal Synthesis of Phosphorus-Rich Transition-Metal Phosphides. *Chem. Mater.* **2008**, *20*, 2618−2620.
(35) Yang, W.; Huang, Y.; Fan, J.; Yu, Y.; Yang, C.; Li, H. A Facile Solution-Phase Synthesis of Cobalt Phosphide Nanorods/Hollow Nanoparticles. *Nanoscale* **2016**, *8*, 4898−4902.
(36) Liu, J.; Meyns, M.; Zhang, T.; Arbiol, J.; Cabot, A.; Shavel, A. Triphenyl Phosphite as the Phosphorus Source for the Scalable and Cost-Effective Production of Transition Metal Phosphides. *Chem Mater* **2018**, *30*, 1799−1807.
(37) Henkes, A. E.; Schaak, R. E. Template-Assisted Synthesis of Shape-Controlled Rh_2P Nanocrystals. *Inorg. Chem.* **2008**, *47*, 671−677.
(38) Henkes, A. E.; Vasquez, Y.; Schaak, R. E. Converting Metals into Phosphides: A General Strategy for the Synthesis of Metal Phosphide Nanocrystals. *J. Am. Chem. Soc.* **2007**, *129*, 1896−1897.
(39) Henkes, E. K.; Schaak, R. E. Trioctylphosphine: A General Phosphorus Source for the Low-Temperature Conversion of Metals into Metal Phosphides. *Chem. Mater.* **2007**, *19*, 4234−4242.
(40) Vasquez, Y.; Henkes, A. E.; Chris Bauer, J.; Schaak, R. E. Nanocrystal Conversion Chemistry: A Unified and Materials-General Strategy for the Template-Based Synthesis of Nanocrystalline Solids. *J. Solid. State. Chem.* **2008**, *181*, 1509−1523.
(41) Xu, J.; Xiong, D.; Amorim, I.; Liu, L. Template-Free Synthesis of Hollow Iron Phosphide−Phosphate Composite Nanotubes for Use as Active and Stable Oxygen Evolution Electrocatalysts. *ACS Appl. Nano Mater.* **2018**, *1*, 617−624.
(42) Xiong, D.; Wang, X.; Li, W.; Liu, L. Facile synthesis of iron phosphide nanorods for efficient and durable electrochemical oxygen evolution. *Chem. Comm.* **2016**, *52*, 8711−8714.
(43) Callejas, J. F.; McEnaney, J. M.; Read, C. G.; Crompton, J. C.; Biacchi, A. J.; Popczun, E. J.; Gordon, T. R.; Lewis, N. S.; Schaak, R. E. Electrocatalytic and Photocatalytic Hydrogen Production from Acidic and Neutral-pH Aqueous Solutions Using Iron Phosphide Nanoparticles. *ACS Nano* **2014**, *8*, 11101−11107.
(44) Mohapatra, J.; Mitra, A.; Tyagi, H.; Bahadur, D.; Aslam, M. Iron oxide nanorods as high-performance magnetic resonance imaging contrast agents. *Nanoscale* **2015**, *7*, 9174−9184.
(45) Adhikari, M.; Singh, A.; Echeverria, E.; McIlroy, D. N.; Vasquez, Y. Iron Pyrite Nanocrystals: A Potential Catalyst for Selective Transfer Hydrogenation of Functionalized Nitroarenes. *ACS Omega* **2020**, *5*, 14104−14110.

(46) Adhikari, M.; Echeverria, E.; Risica, G.; McIlroy, D. N.; Nippe, M.; Vasquez, Y. Synthesis of Magnetite Nanorods from the Reduction of Iron Oxy-Hydroxide with Hydrazine. *ACS Omega* **2020**, *5*, 22440−22448.
(47) Myers, E. C.; Franzen, H. F.; Anderegg, J. W. X-Ray Photoelectron Spectra and Bonding in Transition-Metal Phosphides. *Inorg. Chem.* **1985**, *24*, 1822−1824.
(48) Cho, G.; Kim, H.; Park, Y. S.; Hong, Y.-K.; Ha, D.-H. Phase Transformation of Iron Phosphide Nanoparticles for Hydrogen Evolution Reaction Electrocatalysis. *Int. J. Hydrog. Energy* **2018**, *43*, 11326−11334.
(49) Li, D.; Baydoun, H.; Kulikowski, B.; Brock, S. L. Boosting the Catalytic Performance of Iron Phosphide Nanorods for the Oxygen Evolution Reaction by Incorporation of Manganese. *Chem. Mater.* **2017**, *29*, 3048−3054.
(50) Khanna, P. K.; Jun, K.-W.; Hong, K. B.; Baeg, J.-O.; Mehrotra, G. K. Synthesis of Indium Phosphide Nanoparticles via Catalytic Cleavage of Phosphorus Carbon Bond in N-Trioctylphosphine by Indium. *Mater. Chem. Phys.* **2005**, *92*, 54−58.
(51) Perera, S. C.; Tsoi, G.; Wenger, L. E.; Brock, S. L. Synthesis of MnP Nanocrystals by Treatment of Metal Carbonyl Complexes with Phosphines: A New, Versatile Route to Nanoscale Transition Metal Phosphides. *J. Am. Chem. Soc.* **2003**, *125* (46), 13960−13961.
(52) Ha, D.; Moreau, L. M.; Bealing, C. R.; Zhang, H.; Hennig, R. G.; Robinson, R. D. The Structural Evolution and Diffusion during the Chemical Transformation from Cobalt-to-Cobalt Phosphide Nanoparticles. *J. Mater. Chem.* **2011**, *21*, 11498−11510.
(53) Park, J.; Zheng, H.; Jun, Y.-W.; Alivisatos, A. P. Hetero-Epitaxial Anion Exchange Yields Single-Crystalline Hollow Nanoparticles. *J. Am. Chem. Soc.* **2009**, *131*, 13943−13945.
(54) Muthuswamy, E.; Savithra, G. H. L.; Brock, S. L. Synthetic Levers Enabling Independent Control of Phase, Size, and Morphology in Nickel Phosphide Nanoparticles. *ACS Nano* **2011**, *5*, 2402−2411.
(55) Guo, H.; Chen, Y.; Ping, H.; Jin, J.; Peng, D. Facile Synthesis of Cu and Cu@Cu−Ni Nanocubes and Nanowires in Hydrophobic Solution in the Presence of Nickel and Chloride Ions. *Nanoscale* **2013**, *5*, 2394−2402.

https://doi.org/10.1021/acsnanoscienceau.3c00036
ACS Nanosci. Au 2023, 3, 491−499